Evidence of field-induced nucleation switching in opal: VO_2 composites and VO_2 films

A. B. Pevtsov, A. V. Medvedev, D. A. Kurdyukov, N. D. Il'inskaya, and V. G. Golubev
Ioffe Physical-Technical Institute of the Russian Academy of Sciences, St. Petersburg 194021, Russia

V. G. Karpov
Department of Physics and Astronomy, University of Toledo, Toledo, Ohio 43606, USA
(Received 14 November 2011; published 12 January 2012)

We show that electrical switching in opal-VO_2 composites is governed by the electric field rather than voltage or current. This makes it similar to switching in chalcogenide glasses with the underlying mechanism identified as the field induced nucleation. However, the observed bias dependence of switching delay time is found to be noticeably different from that of standard VO_2 films on "smooth" substrates. This difference is attributed to the disorder effects in polycrystalline structures. The model of field induced nucleation is shown to apply when properly modified to account for that disorder.

DOI: 10.1103/PhysRevB.85.024110 PACS number(s): 64.60.qj, 64.70.Nd, 64.75.St, 84.32.Dd

I. INTRODUCTION

The phenomenon of switching between the insulating and conducting states of VO_2 has been long known[1] and found practical applications in IR imagers,[2] all-optical and electro-optical switches,[3] and modulators.[4] It can be readily triggered by heat since the bulk phase transition between these states takes place at temperature $T_c = 340$ K. Other conceivable triggering factors include electric field,[5] electrostatic or photodoping,[6,7] and stress.[8]

Side by side with the above mentioned phase transition there is a phenomenon of electrical switching in VO_2 films. It is believed to occur nonuniformly in space via conducting filaments that appear in response to strong enough external bias and disappear upon its removal.[9,10] However, the mechanism of such filamentation remains poorly understood. One point of view is that it is due to the electric current generating enough Joule heat to elevate temperature above T_c.[9,11–13] On the other hand, it was proposed that filamentation in VO_2 is similar to the dielectric breakdown in thin oxides.[14] Advocated in this paper is a point of view that filamentation in VO_2 is a largely athermal phenomenon driven by the electric field and it is similar in nature to that in chalcogenide based phase change memory and switches, resistive memory, and thin oxides.

Our investigation here is based on opal-VO_2 composites, which are systems combining properties of three-dimensional (3D) photonic crystals (opal) with a phase changeable component (VO_2) capable of strongly altering its dielectric permittivity.[15] They have been recently considered as prospective materials for ultrafast switching governing the light propagation.[15–17] However, the question of field induced transformations in opal-VO_2 composites compared to normal VO_2 films fabricated by laser ablation remains unanswered. Here the emphasis is on the mechanism of electrical switching in films of opal-VO_2 composites and its relation to that of the standard VO_2 films and other systems capable of switching.

The paper is organized as follows. Section II describes our samples, experimental setup, and results. Section III contains an outline of the field induced nucleation concept (Sec. III A) underlying our interpretation, further developed to account for the closeness to the bulk phase transition in VO_2 (Sec. III B), as well as the effects of disorder in the polycrystalline structure (Sec. III C) and the blocking electrodes (Sec. III D), leading to the predictions of the bias dependent switching delay times in Sec. III E. These predictions are compared to the experimental results in Sec. IV.

II. EXPERIMENT

Our opal-VO_2 samples were fabricated in the form based on $\sim 3\ \mu$m thick films based on the quartz substrates formed by the ten-layer opal structure of a-SiO_2 spheres, diameter of 350 nm each, where ~ 26 % of volume fraction is taken by the interconnected pores. The pores can have either tetrahedral or octahedral shape with the average size of 70 and 140 nm, respectively.

VO_2 synthesis was carried out inside the opal pores. The initial V_2O_5 melt was injected into the pores under capillary forces. The subsequent hydrogenization reduced the composition to VO_2. Both the elemental and phase composition were monitored by energy-dispersive X-ray (EDX) spectroscopy and x-ray diffraction (XRD) techniques before and after reduction.[18] According to our estimates, the pore filling factor does not exceed 50% and can have a moderate gradient toward the top of the film.

The planar gold strip contacts were deposited on the film by explosive lithography, 6 μm apart, as shown in Fig. 1. Figure 2 shows the SEM micrograph of the opal-VO_2 composite surface. It can be seen that the opal pores are filled with VO_2 aggregates. Our earlier x-ray analysis[15] showed that such aggregates in opal-VO_2 composites are composed of finer grains with average size $\sim 30 \pm 2$ nm. The inset in Fig. 2 demonstrates the so-called "inverted opal." Presented in this structure, opal spheres were etched by the fluoric acid. As a result the VO_2 aggregates introduced into opal pores are well seen due to the etching induced high contrast.

Raman measurements of the synthesized opal-VO_2 composites in the same figure demonstrate that opal pores contain nanocrystallites of monoclinic VO_2. As compared to that of nanocrystalline VO_2 film prepared by laser ablation technique, the Raman spectrum of opal-VO_2 composites in Fig. 2 show close similarity.

In our electrical measurements we used a set of generators providing the pulse duration in the range of (10^{-7}–1) s. A

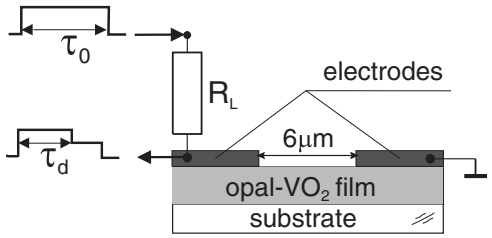

FIG. 1. Sketch of the opal-VO_2 structure (cross section, side view) and the measurement circuitry, R_L is load resistance, τ_0 is duration of voltage pulse applied to sample, and τ_d is delay time of switching due to phase transition in VO_2.

digital storage oscilloscope (Tektronix TDS 2022B) was used to monitor applied voltage before and after switching. In addition, a Peltier element was used to change the sample temperature in the range of $T = 0$ to 40 °C.

Upon application of an electric pulse, the current between electrodes increased abruptly after certain delay (incubation) time τ_d that was found to decrease exponentially with bias. That lead to the decrease of voltage across the device as illustrated in Fig. 3. We note that various pulse forms of Fig. 3

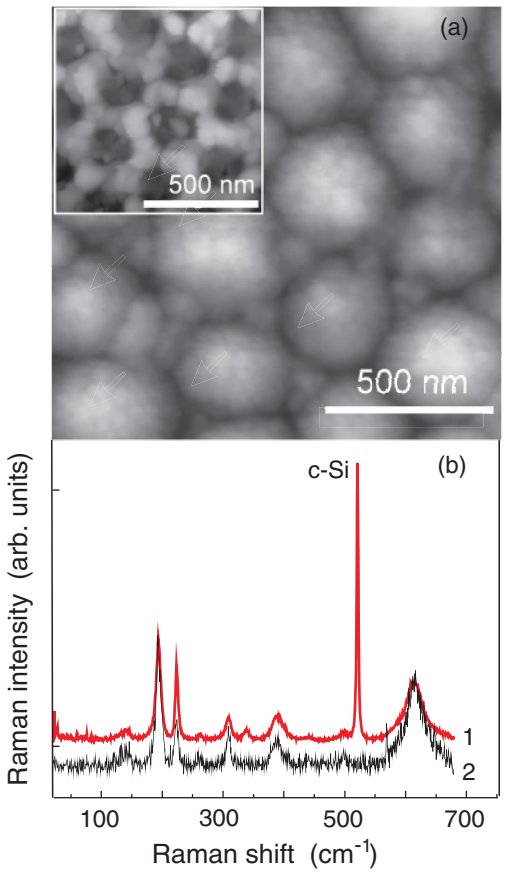

FIG. 2. (Color online) (a) SEM micrograph of the opal-VO_2 film. Opal pores between a-SiO_2 spheres are infiltrated with VO_2 aggregates. Inset: SEM micrograph of opal-VO_2 film with etched opal spheres (inverted opal), light mesh is interconnected VO_2 aggregates, dark regions are air spheres. (b) Raman spectra: crystalline VO_2 film fabricated by laser ablation technique (1), VO_2 in opal pores (2). Strong line marked as c-Si is resulted from Si substrate.

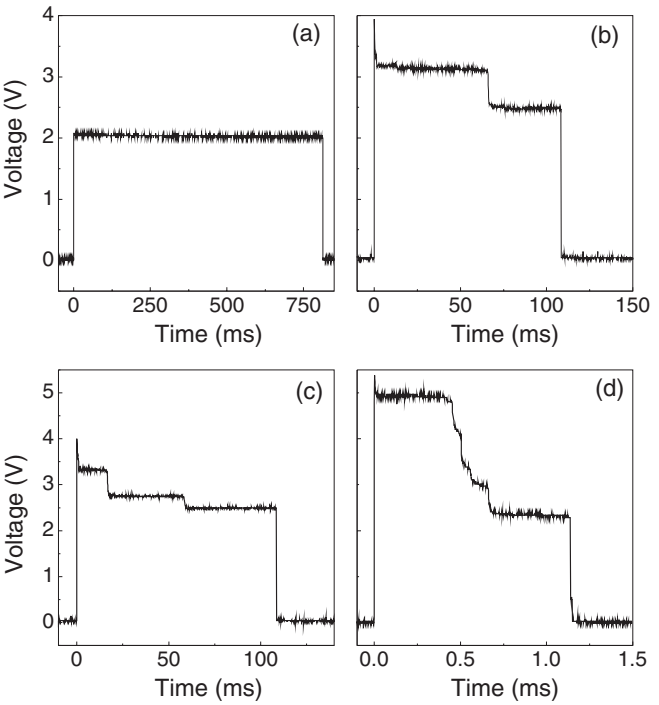

FIG. 3. Representative patterns of the electric pulses showing various switching times. (a) Pulse duration is insufficient for switching (b) Switching at approximately 60 ms triggered by 110 ms long pulse. (c) Two-step switching at ≈20 and ≈60 s triggered by 110 ms long pulse. (d) Multistep switching from ≈0.4 to 0.7 ms triggered by 1.2 ms pulse. The short time overshoots are circuitry related artifact and should not be counted.

were often observed in several subsequent experiments on the same sample. Therefore, the fine details of these forms were not exactly reproducible, while the general trend and range of switching time remained well defined. We attributed the observed voltage changes to the formation of conducting filaments between the electrodes. In some cases, the measured signals demonstrated finer details similar to that observed in Ref. 14 and possibly related to the filament evolution and/or multiple filamentation. In our experiments we used various load resistances R_L and ambient temperatures in order to verify the possibility of temperature driven switching and the role of Joule heat.

Our results are summarized in Fig. 4 along with the published data[20] on electrical switching in VO_2 films on the standard smooth substrates. Our data show that neither the load resistance nor the ambient temperature have significant effect on the observed switching; a similar observation was made earlier in Refs. 14 and 19 for plane VO_2 films. We conclude therefore that the observed switching is most likely field driven, hence falling in the same domain as the recently studied switching in chalcogenide glasses of phase change memory.[21] Another important feature is that while exponential in nature, the bias dependence of switching delay time in VO_2-opal composites is substantially weaker than that measured for the standard VO_2 film.

Following the interpretation of switching in phase change memory,[21] we will describe the observed switching in VO_2 as the field induced nucleation of conducting filaments.

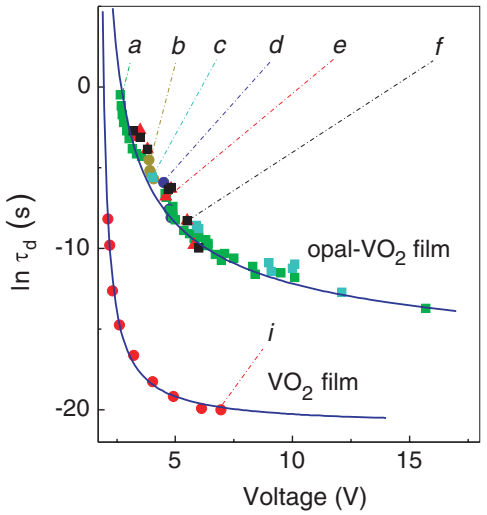

FIG. 4. (Color online) Switching delay time τ_d vs device voltage for standard crystalline VO_2 film (data *i* from Ref. 20) and for opal-VO_2 composites (*a*: $T = 22\,^\circ$C, $R_L = 100\ \Omega$; *b*: $T = 22\,^\circ$C, $R_L = 1000\ \Omega$; *c*: $T = 0\,^\circ$C, $R_L = 100\ \Omega$; *d*: $T = 22\,^\circ$C, $R_L = 5000\ \Omega$; *e*: $T = 7\,^\circ$C, $R_L = 100\ \Omega$; *f*: $T = 40\,^\circ$C, $R_L = 100\ \Omega$). The dispersion in our measurements is reflected in the finite size of the data points. Solid lines represent theoretical fits with Eq. (15) for the case of standard VO_2 film and Eq. (14) for opal-VO_2 composite.

This phenomenological interpretation does not specify the microscopic nature of the conductive phase, yet it enables the description in terms of rather general nucleation theory leading to verifiable predictions.

III. THEORY

A. Field induced nucleation

A conductive, needle-shaped nucleus in an insulating host becomes energetically favorable under strong enough electric field E. The electrostatic energy decrease $F_E = -pE$ is due to the induced electric dipole $p = \alpha E$. The polarizability α of a needle-shaped embryo of length h and radius $R \ll h$ can be estimated as $\alpha \approx \Omega(h/R)^2$, where $\Omega \sim hR^2$ is the volume. This is by factor $(h/R)^2 \gg 1$ greater than that of the equal volume sphere. A more exact expression is given by[22]

$$F_E = -\frac{\varepsilon E^2 \Omega}{8\pi n}, \tag{1}$$

where ε is the electric permittivity of the host insulating phase and the effect of particle geometry is embodied in the depolarizing factor n. For a sphere, $n = 1/3$, $A = 4\pi R^2$, and $\Omega = 4\pi R^3/3$. For a prolate spheroid or cylinder of height H and radius R, the depolarizing factor is[22]

$$n = (R/H)^2[\ln(2H/R) - 1] \equiv (R/H)^2 L. \tag{2}$$

This shows again that for particles of equal volume, the electrostatic contribution is greater for a needle-shaped particle by a huge factor of approximately $(H/R)^2 \gg 1$. The enhancement can be understood by noticing that the induced dipole of a metal needle-shaped particle must be of the order of $p \sim Eh^2$ in order to screen the electric field inside it. While the exact shape of the embryo is not known, approximating it with ellipsoid or cylinder results is rather insignificant in some numerical multipliers, which we neglect in what follows. Along the same lines, we will neglect the weak logarithmic dependence in Eq. (2) approximating the expression in square brackets by unity.

For a mathematically more concise cylinder shape, the free energy is given by $F = A\sigma \pm \Omega|\mu| + F_E$, where σ is the surface tension (so that σA with $A = 2\pi Rh$ is the surface energy), μ is the bulk chemical potential difference (per volume) between the insulating and conducting phases of the material, and we have chosen to use the $\pm$ notation in order to explicitly discriminate between the cases when the bulk conductive phase is more ($\mu < 0$) or less ($\mu > 0$) stable than the insulating one.

We will see that in the latter case, the conductive needle-shaped embryo can still be energetically favorable if the field induced energy decrease [third term in Eq. (3)] is significant. Should that take place, the embryo will disappear upon field removal (unlike the case of $\mu < 0$ where the embryo can exist in zero field). This feature corresponds to the observed switching property.

Taking into account also Eq. (1) the above free energy can be presented in the form

$$F = \frac{W_0}{2}\left(\frac{3Rh}{R_0^2} \pm \frac{3R^2 h}{R_0^3} - \frac{E^2}{E_0^2}\frac{h^3}{R_0^3}\right), \tag{3}$$

where we have introduced the units of the classical nucleation theory[23]

$$W_0 = \frac{16\pi\sigma^3}{3\mu^2}, \quad R_0 = \frac{2\sigma}{|\mu|}, \quad E_0 = 2\left(\frac{W_0}{\varepsilon R_0^3}\right)^{1/2}. \tag{4}$$

They have the meaning of nucleation barrier (W_0) and radius (R_0) for spherical embryos, and E_0 is the characteristic field. These units are convenient (even though we deal with significantly nonspherical particles) because their numerical values are known for the typical material parameters For the typical parameters they are in the range of

$$W_0 \sim 1\ \text{eV}, \quad R_0 \sim 1\ \text{nm}, \quad E_0 \sim 1\ \text{MV/cm}. \tag{5}$$

It is readily seen that the embryo made of metastable bulk conductive phase [+ sign in Eq. (3)] remains energetically favorable when its aspect ratio is large enough,

$$\frac{h}{R} > \frac{E_0}{E}\sqrt{3\left(1 + \frac{R_0}{R}\right)}. \tag{6}$$

In Sec. III B we discuss how these estimates can change in the proximity of the bulk phase transition.

While Eq. (3) formally suggests that needles with $R \to 0$ are most favorable, realistically R must be greater than some minimum value $R_{\min}$ determined by extraneous requirements, such as sufficient conductivity to support a large dipole energy or mechanical integrity. A reasonable $R_{\min}$ is of the order of characteristic interatomic distance,[21] that is, $R_{\min} = \alpha R_0$ with $\alpha \sim 0.1$. In what follows, the dimensionless $\alpha \sim 0.1$ remains a material parameter. Because the field effect cannot be manifested by too thin particles, the free energy in the region $R < R_{\min}$ is substantially larger than described by Eq. (3) and is approximated by a potential wall thereby limiting

possible trajectories of nucleating particles in the (R,h) space to $R > R_{\min}$.

With the latter in mind, the nucleation barrier corresponding to free energy in Eq. (3) is given by[21]

$$W = W_0 \alpha^{3/2} \frac{E_0}{E} \tag{7}$$

with the associated critical aspect ratio $h_c/R_{\min} = E_0/(E\alpha^{1/2}) \gg 1$. It is significantly suppressed when $E > E_0\alpha^{3/2}$. Correspondingly, nucleation of needle-shaped particles dominates over that of spherical particles.

Since created, the conductive needle-shaped embryo acts as a metal rod focusing the electric field and triggering further nucleation events. This leads to a conductive filament shorting the system. The primary nucleation remains a bottleneck setting the delay time $\tau_d = \tau_0 \exp(W/kT)$ with W of Eq. (7), which we identify with the observed switching time.

B. Field induced nucleation in the proximity of bulk phase transition

To account for the bulk phase transition at $T_c = 340$ K in VO_2, one can use the standard approximation $\mu = \mu_0(1 - T/T_c)$, where μ_0 is the chemical potential difference between the two phases at zero temperature. This will result in the corresponding renormalization, according to which the parameters in Eq. (4) will be replaced respectively with the following:

$$\frac{W_0}{(1 - T/T_c)^2}, \quad \frac{R_0}{1 - T/T_c}, \quad E_0|1 - T/T_c|^{1/2}. \tag{8}$$

Because $R_{\min}$ is determined by microscopic structure and remains practically independent of temperature, we observe that $\alpha \propto (1 - T/T_c)$. Taking into account the latter scaling relations, Eq. (7) predicts that the nucleation barrier W is temperature independent. This conclusion is in striking difference with the prediction of classical nucleation theory that the nucleation barrier for for spherical embryos is strongly temperature dependent,

$$W_0 \propto \mu^{-2} \propto (1 - T/T_c)^{-2}. \tag{9}$$

It is readily seen from the above that the field induced nucleation of needle-shaped embryos becomes exponentially more effective than the classical nucleation of spherical particles in the proximity of bulk phase transition. Indeed, the latter is characterized by the barrier that can be presented as $W_0 = W_{00}(1 - T/T_c)^{-2}$ while the temperature independent field induced nucleation barrier can be presented in the form $W = W_{00}\alpha_{00}^{3/2}E_{00}/E$, where W_{00}, E_{00}, and α_{00} refer to zero temperature. As a result, the field induced nucleation can dominate already under relatively weak fields $E > E_{00}\alpha_{00}^{3/2}(1 - T/T_c)^2$. Here the characteristic values of "zero temperature" quantities W_{00}, E_{00}, and α_{00} far from the bulk phase transition are estimated in Eq. (5).

Quantitatively this effect can be rather substantial as $1 - T/T_c \approx 0.2$ for the case of VO_2 at room temperature. Substituting here the above mentioned numerical numerical values yields $E > 100$ V/cm. Simply stated, the field induced nucleation dominates in the proximity of bulk phase transitions; the required electric fields can be either externally applied, say, in the form of low power laser beam, or generated internally as a result of minute material nonuniformities.

We note in this connection that needle-shaped nuclei in VO_2 have been observed indeed.[24] In the terms of field induced nucleation, that observation could be attributed to the local electric fields generated by the grain boundaries in the polycrystalline structure of VO_2.

C. Effects of disorder

Structural disorder can have an exponentially strong effect on nucleation rate[25,26] including the case of field induced nucleation.[27] This effect is due to the randomness of nucleation barriers in a disordered system leading to a broad dispersion of the observed nucleation times. In particular, "weak" local regions with lower than average nucleation barriers give rise to abnormally fast nucleation events.

Here we consider another disorder related mechanism that is due to the distribution of local electric fields across the system, which significantly changes the above discussed result in Eq. (7). This mechanism is a consequence of the polycrystalline structure of VO_2. Characteristic of such a structure are random potential barriers associated with grain boundaries. These random barriers have exponentially different electrical resistances. The electric currents flowing through these random barriers will generate a broad distribution of electric potentials across them as illustrated in Fig. 5(a). The latter give rise to a broad distribution of local electric fields. The larger than average local fields in that distribution will lead to the accelerated field induced nucleation.

Following the above reasoning, consider a transversal electric current pathway through the structure as a series of $L/l_0 \gg 1$ random resistors, $R_1 > R_2 > R_3 \cdots$. Here L is the distance between the device electrodes, and l_0 is the linear size of one such a resistor, of the order of the average diameter of the VO_2 grains. In this series, the largest voltage drop is across the highest resistor R_1.

If the resistors were purely ohmic, then the major portion of the applied voltage would drop across the resistor R_1. However

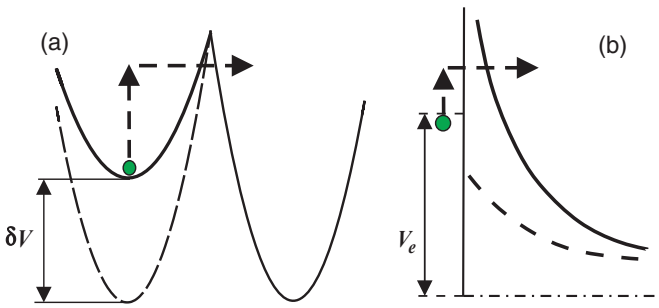

FIG. 5. (Color online) Voltage distribution across potential barriers determining the transversal electron transport through a polycrystalline switching structure. Fat dash arrows represent the partially activated electronic transitions facilitated by the barrier accumulated voltages. (a) Voltage δV accumulated at the grain boundary barrier; dashed line represents the grain boundary potential under zero voltage. (b) Voltage V_e accumulated at the blocking electrode barrier between a metal (to the left of vertical line) and VO_2. Dashed line shows the barrier under zero voltage. Dash-dot lines show the Fermi levels in the metal and VO_2.

the voltage distribution is strongly affected by the resistors significant nonohmicity typical of the barrier structures. The mechanisms of such nonohmicity can vary between different systems; examples are the Pool-Frenkel effect,[28] electric charge redistribution,[29] local heating, etc.

The nonohmicity will generally suppress the resistances in the series starting with that of R_1. As soon as the highest resistance R_1 is suppressed down to the level of R_2, most of the applied voltage becomes distributed between the resistors R_1 and R_2. This will further suppress these resistances down to the level of R_3, etc. Continuing along these lines, the entire voltage V will be eventually distributed among a large number of elements $L/l_0 \gg 1$ in such a way that the least resistive of them will bear a relatively small portion $\delta V_{\min}$ of the total potential.

The highest voltage drop in the above the series $\delta V_{\max}$ can be estimated from the condition

$$\frac{L}{l_0}\int_{\delta V_{\min}}^{\delta V_{\max}} \delta V \frac{d\delta V}{\Delta} = V. \tag{10}$$

Here we have assumed that the probabilistic distribution of voltage drops across the random elements in the series has the simplest possible form: it is uniform, with width Δ; the latter remains an unknown parameter in the present context. The case of strong disorder implies at least $\Delta \gg kT$.

Assuming that $V_{\max}$ is significantly greater than $V_{\min}$, one can neglect the low limit contribution in the integral of Eq. (10), which leads to the following estimate of the strongest local electric field in the series:

$$E_{\max} = \frac{\delta V_{\max}}{l_0} = \sqrt{\frac{2V\Delta}{l_0 L}}. \tag{11}$$

This field should be used in place of E in Eq. (7). Equation (11) predicts that the above mechanism suppresses the nucleation barrier of field induced nucleation ($E_{\max} > V/L$) when

$$2L/l_0 > V/\Delta. \tag{12}$$

The latter inequality can obey for realistic $V \sim 1$ V, $\Delta \gg kT$, and $L/l_0 \gg 1$. Because given the total electric potential drop across the structure implies that $E_{\max} < V/L$ we conclude that the inequality in Eq. (12) is a necessary condition for the above mechanism to work. Note that the enhancement ratio of the maximum over the average field can be rather substantial,

$$\frac{E_{\max}}{\langle E\rangle} = \sqrt{\frac{L\Delta}{l_0 V}} \gg 1 \tag{13}$$

when $L \gg l_0$. For example, assuming $\Delta \sim 1$ V, $V \sim 1$–10 V (in connection with the data in Fig. 4), and $L/l_0 \sim 10^2$–10^4 yields $E_{\max}/\langle E\rangle \sim 10$–$100$.

A comment is in order regarding the above concept of local field enhancement. It applies only in the case when the current flow has to overcome the highest resistors in the system. Along the lines of the standard percolation theory that happens when the system dimensions, particularly the length of the current pathways, are large enough exceeding the corresponding correlation radius of the percolation network. To the contrary, for the case of transverse conduction through disordered thin films, the current can flow through the easiest pathways,[30,31] in which case the strongest field is of the order of its average value.

D. Role of device electrodes

The analysis in Sec. III C implied the electric current flow governing the distribution of the electric field through the system. That is tantamount to the inequality $\tau_d \gg \tau_M$ between the nucleation time τ_d and the Maxwell (dielectric) relaxation time τ_M, that is, electric currents having enough time to reach steady state before the nucleation takes place. The fast electric relaxation requires, in particular, that the electrodes do not exert strong blocking action upon the current flow. With the typical blocking electrodes used in switching devices this is achieved by placing a significant voltage drop V_e across the electrodes in order to exponentially increases the electrode transparency,[32–34] as illustrated in Fig. 5(b). The value of V_e is typically of the order of 1 V; it is kept as a fitting parameter for the purposes of this paper.

E. Bias dependent nucleation time

Taking into account all the above consideration, the voltage dependence of switching time $\tau_d = \tau_0 \exp(W/kT)$ for uniform systems can be presented in the form

$$\tau_d = \tau_0 \exp\left[\frac{W_0\alpha^{3/2}E_0 L}{kT(V - V_e)}\right]. \tag{14}$$

However it takes the following form for the system with strong disorder:

$$\tau_d = \tau_0 \exp\left[\frac{W_0\alpha^{3/2}E_0 l_0^{1/2}L^{1/2}}{kT(2\Delta)^{1/2}(V - V_e)^{1/2}}\right]. \tag{15}$$

These equations were used to fit the data in Fig. 4.

IV. DISCUSSION AND CONCLUSIONS

Generally, Eqs. (14) and (15) are overly flexible: it was found that either one can be used to formally fit the data by properly adjusting their corresponding parameters in

$$\ln\tau_d = P_1 + \frac{P_2}{V - P_3} \quad \text{and} \quad \ln\tau_d = P_1' + \sqrt{\frac{P_2'}{V - P_3'}}, \tag{16}$$

Therefore, the interpretation critically depends on the numerical values of fitting parameters and their relevance to the above theoretical predictions. We note in particular a useful relation

$$P_2' = \frac{P_2^2}{2\Delta}\frac{l_0}{L}. \tag{17}$$

In deciding between the above two equations, a significant difference between the geometries of structures used in Ref. 20 and that of the present work needs to be taken into account. The former used $L = 0.2$ mm long, 5–10 μm wide, 0.1–1 μm thick bridge-like VO_2 films between two Al electrodes. To the contrary, the present work experiments were carried out on $L = 6$ μm long, $\sim$1 mm wide, $\sim$3 μm thick slit-like opal-VO_2 composites. In view of these numerical values, the important fact reflected in Fig. 4 is that, under the same voltages V, the

former structures showed considerably shorter switching time in spite of the much lower average electric fields $\langle E\rangle = V/L$.

Our interpretation of the above fact is that it is due to the much stronger nonuniformity effects in the long structures of Ref. 20 leading to very strong local fields [cf. Eq. (11)]. Therefore the data of Ref. 20 correspond to Eq. (15). Taking into account the interpretation at the end of Sec. III C, we assume then that the samples dealt with in the present paper are thin enough to have multiple "shunting" paths determining their transversal conduction; hence the first of Eqs. (16) corresponding to Eq. (14) is more appropriate.

This approach returns the following fitting parameters: $P_1 = -16 \pm 1$, $P_2 = 39 \pm 1$, $P_3 = 0 \pm 0.2$ for our original data, and $P_1^{'} = -23 \pm 2$, $P_2^{'} = 53 \pm 4$, $P_3^{'} = 1.9 \pm 0.1$ for the data of Ref. 20. Based on the sample length ratio 0.2 mm/(6 μm)$\approx$ 30 and assuming a rough estimate $\Delta \sim$ 1 V, we have used Eq. (17) to check the adequacy of our interpretation. We have taken into account that Eq. (17) relates the parameters corresponding to the same distance L between the contacts. When the two distances are different, the right-hand side of Eq. (17) must be multiplied by their ratio of 30. This enables one to estimate $l_0/L \sim 2 \times 10^{-3}$, where $L = 6\,\mu$m, and thus the VO_2 grain size: $l_0 \sim 10$ nm. The latter is consistent with the experimental estimates of the VO_2 grain sizes in Ref. 24 and with the x-ray data on VO_2 grains in opal pores,[15] thus rendering certain credibility to our interpretation.

The difference between P_3 and $P_3^{'}$ can be attributed to the electrode materials used in Ref. 20 (Al) and in our work (Au) and pointing toward Au forming nonblocking electrodes with VO_2. On the other hand, the difference between P_1 and $P_1^{'}$ can be due to the effects of electronic excitations in Ref. 20 using Si substrate and our work where the substrate was SiO_2.

Multistep switching in Fig. 3 presents another observation consistent with our interpretation. Indeed, in the planar slit-like structure used in our experiments, switching can only be observable if it takes place in one of the "shunting" current pathways determining the voltage across VO_2 strip. In the regime of current source, switching in every other "shunting" pathway will subsequently contribute to the observed voltage drop. We note that similar multistep switching and switching time range were observed in the earlier work using slit-like VO_2 samples deposited on smooth Al_2O_3 substrate,[14] where these current paths were identified by optical microscopy. The microscopic nature of multiple switching in our samples remains an open question.

We note that our observations did not reveal any significant temperature dependence of switching times, which is fully consistent with the predictions of the field induced nucleation model in Sec. III B. Indeed, according to Eq. (9) the classical theory of phase transitions predicts very strong temperature dependence $\ln \tau_d \propto (1 - T/T_c)^{-2}$ regardless of the microscopic nature of the underlying structural transformation. This predicts the change of approximately 7 in $\ln \tau_d$ between our probed temperatures of 0 and 40 °C, which has not been observed. To the contrary, the field induced nucleation model predicts only small temperature changes $\ln \tau_d \propto 1/T$, well within the range of statistical fluctuations in our experiments.

In conclusion, we have reported the results of our experimental study of switching phenomena in opal-VO_2 composite films. Measurements were conducted over long read pulses for a range of applied voltages and load resistances. In addition, we have proposed a theory rendering a quantitative interpretation of our and some published observations. Several of our key results are listed below.

(a) Switching times in opal composite films depend exponentially on applied bias and is independent on the electric current and actual temperature range.

(b) Relevant theory of field induced nucleation was developed and verified by fitting of experimental data.

(c) Thus experimental and theoretical results provide evidence of field induced nucleation of conducting paths being a mechanism of switching in VO_2 films and opal-VO_2 composites.

Finally, we note that our work leaves the microscopic aspects of switching in VO_2 largely unspecified. In particular, the models of electronic or photodoping, or stress induced transformations can be accounted for in our interpretation by introducing the corresponding dependencies of the nucleation parameters, for example, chemical potential μ and/or surface energy σ dependent on the charge carrier concentration, etc.

ACKNOWLEDGMENTS

The authors are grateful to Yu. Zadiranov and A. Lutetskiy for help with sample preparation. This work was partially supported by the Russian Academy of Sciences.

[1] F. J. Morin, Phys. Rev. Lett. **3**, 34 (1959).
[2] W. Bruckner, H. Opperman, W. Reicheld, E. I. Terukov, F. A. Tschudnovskii, and E. Wolf, *Vanadium Oxide* (Akademy, Berlin, 1983), p. 251.
[3] M. Soltani, M. Chaker, E. Haddad, and R. Kruzelesky, Meas. Sci. Technol. **17**, 1052 (2006).
[4] R. M. Briggs, I. M. Pryce, and H. A. Atwater, Opt. Express **18**, 11192 (2010).
[5] H.-T. Kim, B.-G. Chae, D.-H. Youn, G. Kim, K.-Y. Kang, S.-J. Lee, K. Kim, and Y.-S. Limb, Appl. Phys. Lett. **86**, 242101 (2005).
[6] M. M. Qazilbash, Z. Q. Li, V. Podzorov, M. Brehm, F. Keilmann, B. G. Chae, H. T. Kim, and D. N. Basov, Appl. Phys. Lett. **92**, 241906 (2008).
[7] A. Cavalleri, Cs. Toth, C. W. Siders, J. A. Squier, F. Raksi, P. Forget, and J. C. Kieffer, Phys. Rev. Lett. **87**, 237401 (2001); A. Cavallery, M. Rini, and R. W. Schoelten, J. Phys. Soc. Jpn. **75**, 011004 (2006).
[8] J. P. Pouget, H. Launois, J. P. D'Haenens, P. Merenda, and T. M. Rice, Phys. Rev. Lett. **35**, 873 (1975); J. I. Sohn, H. J. Joo, D. Ahn, H. H. Lee, A. E. Porter, K. Kim, D. J. Kang, and M. E. Welland, Nano Lett. **9**, 3392 (2009).
[9] J. Duchene, M. Terraillon, P. Paily, and G. Adam, Appl. Phys. Lett. **19**, 115 (1971).
[10] B.-J. Kim, Y. W. Lee, B.-G. Chae, S. J. Yun, S.-Y. Oh, and H.-T. Kim, Appl. Phys. Lett. **90**, 023515 (2007).
[11] J. S. Lee, M. Ortolani, J. Kouba, A. Firsov, Y. J. Chang, T. W. Noh, and U. Schade, Infrared Phys. Technol. **51**, 443 (2008).

[12]J. S. Lee, M. Ortolani, U. Schade, Y. J. Chang and T. W. Noh, Appl. Phys. Lett. **91**, 133509 (2007).
[13]J. S. Lee, M. Ortolani, U. Schadea, Y. J. Chang and T. W. Noh, Appl. Phys. Lett. **90**, 051907 (2007).
[14]K. Okimura, N. Ezreena, Y. Sasakawa, and J. Sakai, Jpn. J. Appl. Phys. **48**, 065003 (2009).
[15]V. Yu. Davydov, N. F. Kartenko, D. A. Kurdyukov, A. V. Medvedev, A. B. Pevtsov, A. V. Scherbakov, and E. B. Shadrin, Appl. Phys. Lett. **79**, 2127 (2001).
[16]D. Mazurenko, R. Kerst, J. I. Dijkhuis, A. V. Akimov, V. G. Golubev, A. A. Kaplyanskii, D. A. Kurdykov, and A. B. Pevtsov, Appl. Phys. Lett. **86**, 041114 (2005).
[17]A. B. Pevtsov, D. A. Kurdyukov, V. G. Golubev, A. V. Akimov, A. A. Meluchev, A. V. Sel'kin, A. A. Kaplyanskii, D. R. Yakovlev, and M. Bayer, Phys. Rev. B **75**, 153101 (2007).
[18]D. A. Kurdyukov, S. A. Grudinkin, A. V. Nashchekin, A. N. Smirnov, E. Yu. Trofimova, M. A. Yagovkina, A. B. Pevtsov, and V. G. Golubev, Phys. Solid State **53**, 428 (2011).
[19]B.-G. Chae, H.-T. Kim, D.-H. Youn, and K.-Y. Kang, Physica B **369**, 76 (2005).
[20]G. Stefanovich, A. Pergament, and D. Stefanovich, J. Phys. Condens. Matter **12**, 8837 (2000).
[21]V. G. Karpov, Y. A. Kryukov, I. V. Karpov, and M. Mitra, Phys. Rev. B **78**, 052201 (2008); I. V. Karpov, M. Mitra, G. Spadini, U. Kau, Y. A. Kryukov, and V. G. Karpov, Appl. Phys. Lett. **92**, 173501 (2008); M. Nardone, V. G. Karpov, C. Jackson, and I. V. Karpov, *ibid.* **94**, 103509 (2009); V. G. Karpov, *ibid.* **97**, 033505 (2010).
[22]L. D. Landau, I. M. Lifshitz, and L. P. Pitaevskii, *Electrodynamics of Continuous Media* (Elsevier, New York, 1984).
[23]L. D. Landau and E. M. Lifshitz, *Statistical Physics* (Pergamon, Oxford, 1980); D. Kaschiev, Cryst. Res. Technol. **38**, 555 (2003).
[24]R. Lopez, L. A. Boatner, T. E. Haynes, L. C. Feldmanb, and R. F. Haglund Jr., J. Appl. Phys. **92**, 4031 (2002); R. Lopez, T. E. Haynes, L. A. Boatner, L. C. Feldman, and R. F. Haglund Jr., Phys. Rev. B **65**, 224113 (2002).
[25]A. B. Pevtsov, V. Yu. Davydov, N. A. Feoktistov, and V. G. Karpov, Phys. Rev. B **52**, 955 (1995).
[26]V. G. Karpov and David W. Oxtoby, Phys. Rev. B **54**, 9734 (1996).
[27]V. G. Karpov, Y. A. Kryukov, I. V. Karpov, and M. Mitra, J. Appl. Phys. **104**, 054507 (2008).
[28]R. M. Hill, Philos. Mag. **23**, 59 (1971); J. Frenkel, Phys. Rev. **54**, 657 (1938); H. H. Poole, Lond. Edinb. Dubl. Philos. Mag. **33**, 112 (1916); **34**, 195 (1917).
[29]B. I. Shklovskii, Fiz. Techn. Poluprovodn. **6**, 2355 (1972) [Sov. Phys. Semicond. **6**, 1964 (1973)]; E. I. Levin, I. M. Ruzin, and B. I. Shklovskii, Fiz. Tekh. Poluprovodn. **22**, 642 (1988) [Sov. Phys. Semicond. **22**, 401 (1988)].
[30]M. Pollak and J. J. Hauser, Phys. Rev. Lett. **31**, 21 (1973).
[31]M. E. Raikh and I. M. Ruzin, in *Mesoscopic Phenomena in Solids*, edited by B. L. Altshuller, P. A. Lee, and R. A. Webb (Elsevier, New York, 1991), p. 315.
[32]H. Fritzsche, J. Phys. Chem. Solids **68**, 878 (2007).
[33]K. E. Petersen and D. Adler, J. Appl. Phys. **50**, 5065 (1979).
[34]V. G. Karpov, M. Nardone, and M. Simon, J. Appl. Phys. **109**, 114507 (2011).